NANO LETTERS

Letter

pubs.acs.org/NanoLett

Grain Boundary Engineering for Improved Thin Silicon Photovoltaics

Rajamani Raghunathan,[†] Eric Johlin,[‡] and Jeffrey C. Grossman*,[†]

[†]Department of Materials Science and Engineering and [‡]Department of Mechanical Engineering, Massachusetts Institute of Technology, 77 Massachusetts Avenue, Cambridge, Massachusetts 02139, United States

Supporting Information

ABSTRACT: In photovoltaic devices, the bulk disorder introduced by grain boundaries (GBs) in polycrystalline silicon is generally considered to be detrimental to the physical stability and electronic transport of the bulk material. However, at the extremum of disorder, amorphous silicon is known to have a beneficially increased band gap and enhanced optical absorption. This study is focused on understanding and utilizing the nature of the most commonly encountered Σ_3 GBs, in an attempt to balance incorporation of the advantageous properties of amorphous silicon while avoiding the degraded electronic transport of a fully amorphous system. A combination of theoretical methods is employed to understand the impact of ordered Σ_3 GBs on the material properties and full-device photovoltaic performance.

	c-Si	a-Si:H	GBE-Si
Gap (eV)	1.17	1.68	1.38
Optical Abs.	Poor	Good	Good
Mobility	Good	Poor	Good

KEYWORDS: *Photovoltaics, grain boundary engineering, density functional theory, silicon*

In 2012, crystalline (c-Si) silicon composed the active layer of 89% of photovoltaic (PV) modules produced worldwide, with thin film (generally amorphous) silicon (a-Si:H) accounting for an additional 4%.[1] As is well-established, while the electron and hole mobilities of c-Si are quite high, the material suffers from poor optical absorption and a suboptimal, indirect band gap. In a-Si:H, the situation is reversed—the optical absorption is significantly increased relative to c-Si due to its direct HOMO−LUMO gap,[2] but the low hole mobility limits the cell performance.[3] Additionally, the Stabler−Wronski effect, a light-induced degradation mechanism, reduces cell efficiencies further, by 10% to 30% within a few days of sun exposure.[4,5] Nano(and micro)crystalline silicon (both referred to as nc-Si here, for simplicity) attempt to strike a beneficial balance between amorphous and crystalline silicon, maintaining most of the increased absorption and band gap of a-Si:H[6] while improving upon the carrier mobilities toward those of c-Si.[7] Despite the potential of such an approach, nc-Si device efficiencies still remain below those of either a-Si:H or c-Si.[8] While nc-Si represents an attempt to move the deficient properties of a-Si toward those of c-Si, the limited performance of the material along with the fact that the best nc-Si devices occur at low crystalline volume fractions indicate that this approach may not be feasible.[9−11] In contrast to the case of nc-Si (introducing order into a disordered system), the opposite approach of introducing disorder into an otherwise-crystalline material, has received far less attention. It has been observed elsewhere that the introduction of disorder in the form of a combination of GBs and Cl doping in polycrystalline CdTe creates charge inversion at the interface, aiding majority carrier transport within the conducting GB channels and minority carrier transport outside the GB core, improving the solar cell performance of poly- over mono-crystalline devices.[12−14] However, the presence of GBs in polycrystalline silicon not only creates recombination centers in the form of deep-level defect states, thereby reducing carrier lifetimes significantly, but also reduces the overall carrier mobility by creating potential barriers for charge transport. One possibility of overcoming these harmful influences of GBs is by introducing controlled disorder in silicon, leveraging the diversity of GB orientations and misfit angles already present in polycrystalline materials. However, in order to achieve beneficial effects of GBs in silicon, it would be necessary to choose suitable GBs and orient them in such a manner as to improve the optical absorption and bandgap (toward those of a-Si:H) without substantial degradation of the superior transport properties of c-Si, and demonstrate that these properties combine into full device-scale PV efficiency improvements.[15]

Of the numerous types of GBs possible in a polycrystalline material, experiments and theoretical models show that Σ_3, Σ_9, and Σ_{27} GBs are energetically favored in polycrystalline silicon; in particular Σ_3 GBs are most frequently encountered.[16,17] Thanks to the recent advancements in grain boundary engineering (GBE) techniques like unidirectional and rotational solidification, thermomechanical processing of deformed solid phase and crystallization from the solid phase, it is now possible to incorporate GBs with a specific character into a material.[18−20] This has led to numerous studies related to the energetics, atomic and electronic structure, and defect physics in semiconductor GBs, with emphasis on understanding the impact of these properties on electronic transport.[21−26] However, in order to answer the question of whether GBE

Received: March 18, 2014
Revised: June 12, 2014
Published: June 25, 2014

 © 2014 American Chemical Society

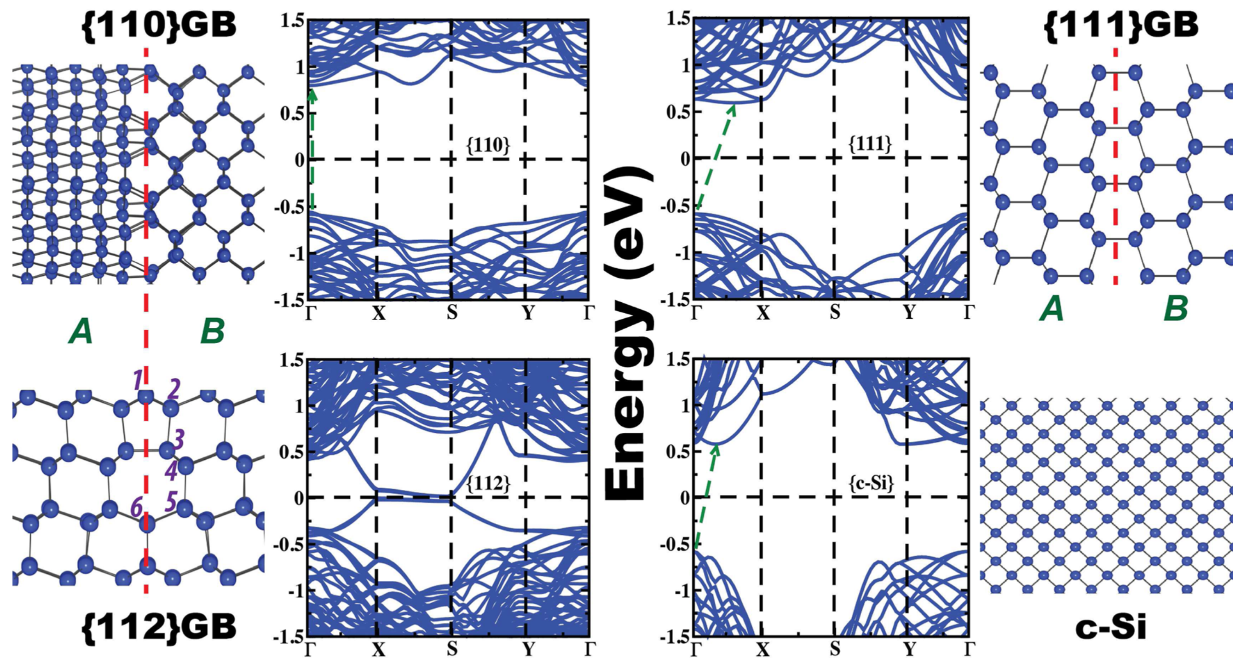

Figure 1. Atomic and electronic structures of (top left) {110}, (top right) {111}, (bottom left) {112} GBs, and (bottom right) c-Si. The GB interfaces are marked by dashed lines. The regions marked A and B form the crystalline regions or grains. In the band structure plots the Fermi energy is at zero, and the dashed green lines indicate the band gap.

could be beneficial to PV, both the electronic and optical properties must be understood and simultaneously optimized.

In this work, density functional theory (DFT) is employed to characterize Σ_3 coincidence site lattice GBs in silicon and to predict which of these GBs may be beneficial to solar energy conversion. Using our computed band structures and optical absorption coefficients we show that, depending on the interface atomic structure, particular GBs can exhibit either significantly higher or lower optical absorption relative to c-Si throughout the visible spectrum, as well as modified band gaps. We further compute the electronic conductivities, σ, using a Boltzmann transport approach to assess the impact of such GBs on charge transport. These results are combined into a finite element model to predict energy conversion efficiencies of GBE solar cells, where it is shown that significant enhancements in energy conversion efficiency over c-Si may be possible for thin device configurations.

Methodology. The starting Σ_3 GB structures were obtained using the *GB Studio* program.[27] The coincidence site lattice GB structures consist of two crystal-like regions or grains (A and B), which form an interface along a chosen crystallographic plane, {110}, {111}, or {112} (see Figure 1). The grains A and B are misoriented with respect to one another by an angle Ω, either parallel to the GB interface (as in the {111} and {112} tilt GBs) or perpendicular to the GB surface (as in the {110} twist boundary). The tetragonal supercell was repeated in all three directions using periodic boundary conditions (PBC). Each supercell contains two GBs, one in the middle of the supercell and the other due to the PBC along the direction normal to the GB plane.

First-principles calculations were performed within the framework of DFT using the Vienna ab initio simulation program.[28] The projector-augmented wave method with the generalized gradient approximation PBE (GGA-PBE) was used for the exchange-correlation potential.[29−32] A plane wave basis cutoff energy of 350 eV and well-converged k-point mesh of ($4 \times 4 \times 4$) were used in all calculations. All structures were allowed to relax until the forces acting on each atom were less than 0.01 eV/Å. The fully relaxed structures were used to compute the electronic band structure. In order to gain a qualitative understanding of optical absorption of GBE materials, the absorption coefficients were obtained from the imaginary part of the dielectric constants computed from DFT within the random phase approximation (RPA). The room temperature (300 K) electronic conductivities for n and p type structures were computed by employing the Boltzmann transport equation within the constant relaxation time approximation using the energy eigenvalues obtained from DFT, as this approach is known to accurately describe the electronic properties of metals and semiconductors.[33−38] In order to obtain converged results we used a dense k-point mesh containing 68 points in the irreducible Brillouin zone. The principal components of electronic conductivity, σ_x, σ_y, and σ_z, were obtained by diagonalizing the conductivity tensor Σ computed from the relation

$$\Sigma = e^2\tau \sum_n \int \frac{d\mathbf{k}}{4\pi^3}\left(-\frac{\partial f(\epsilon_{nk})}{\partial \epsilon_{nk}}\right)\mathbf{v}_{nk}\mathbf{v}_{nk} \tag{1}$$

where e is the electronic charge, τ is the relaxation time, $\mathbf{k}$ is the reciprocal lattice vector, ϵ_{nk} is the energy eigenvalue of the nth band at wavevector $\mathbf{k}$ (DFT eigenvalues), $f(\epsilon_{nk})$ is the Fermi−Dirac function at a given temperature, and $\mathbf{v}_{nk} = (1/\hbar)\nabla_k\epsilon_{nk}$.[39] The value of τ was chosen based on previous far-infrared reflectance spectra studies on phosphorus doped silicon in the concentration range 10^{17}−10^{18} cm^{-3}.[40] We further confirmed that the computed conductivity values for c-Si match well with that reported by Weber and Gmelin.[41] The same relaxation time was used in our calculations for {110} and {111} GBs as well, which is reasonable since our computed charge density of valence and conduction bands showed "bulk" like character and we do not expect any recombination centers. We note that

scattering by phonons at the interface is not included in this present study, although this is likely to represent a small effect since we are using GBs with high symmetry. Finite-element device modeling was performed using *COMSOL* with light absorption and carrier generation simulated by solving the Helmholtz wave-optics equation and the diffusion of charged species in the material simulated using a drift-diffusion model. More details about the methodology can be found in the Supporting Information.

Atomic Structure. The grain boundary formation energies (E_{GB}) for the relaxed structures were obtained using $E_{GB} = (E_{GBS} - E_{Bulk})/2S$, where E_{GBS} is the energy of the relaxed structure with GB, E_{Bulk} is the energy of bulk c-Si with no GBs, but containing the same number of Si atoms, S is the GB surface area, and the factor of 2 comes from the supercell containing two grain boundaries. The number of unit cells inside grains A and B along the direction normal to the GB plane was increased until the E_{GB} values were converged to less than 10^{-3} eV/Å^2, in order to eliminate any interaction between the neighboring GBs. Convergence was achieved for structures with separation between the neighboring GBs greater than 3 nm. The GB energies showed that {111} (E_{GB} = 0.001 eV/Å^2) is the most favorable GB, with negligible deviation from the ideal silicon tetrahedral structure. The GB energies for {110} and {112} structures were found to be 0.040 eV/Å^2 and 0.042 eV/Å^2, respectively, suggesting extensive rearrangement of atoms at the interface. This was further confirmed from the calculated bond length and bond angle distributions in the relaxed structures which showed that the {112} GB cores contain highly strained bonds (see Supporting Information). In addition, the {112} GB contains 5-fold coordinated silicon atoms, indexed by “1”, as shown in Figure 1. The 5-fold coordinated atoms in the {112} GB are associated with four highly strained bonds of length ≈2.55 Å (corresponding to an 8% increase over the ideal Si−Si bond length) and a fifth unstrained bond of length 2.37 Å. Thus, we expect defect levels highly localized around the dislocation core in the electronic structure of a {112} GB. While such strained bonds are completely absent in the {111} GB, the {110} structure possesses a small number of bonds with less than 3% compressive strain. Neither {111} nor {110} GBs however show any under- or overcoordinated silicon atoms. The relaxed GB structures as well as the computed GB energies are consistent with previously reported GB structures using HRTEM results and DFT.[42,43]

Electronic Band Structure. As mentioned, our GB structures contain multiple unit cells in each direction in order to describe the GB interface adequately and also to avoid direct interaction between the neighboring GBs. Such periodic supercell treatments can often lead to folding of energy bands though they do not alter the fundamental energy gap (a more detailed description of zone folding can be found in the SI). Zone folding poses a challenge to the analysis of the electronic structures of extended supercells and has already been previously reported in semiconducting nanostructures such as silicon and germanium nanotubes, nanowires, and quantum slabs.[44−48] Though the unfolded band structure can be reconstructed from zone-folded band structures, the goal of this work is to understand the fundamental energy gaps in GB engineered structures,[49,50] and thus such reconstruction is not considered here.

The GGA-PBE band structures of GB structures along different symmetry directions in a tetragonal Brillouin zone are shown in Figure 1, together with that of a single-crystal silicon supercell containing the same number of atoms for comparison. The conduction bands of the semiconducting structures, namely, the {110} and {111} GBs, and c-Si, are scissor-shifted by 0.57 eV to match the experimental band gap E_g = 1.17 eV of c-Si. This correction term is widely employed to account for quasi-particle energy corrections in silicon.[46,51,52] It is however not applied to the {112} GB system since it shows metallic behavior unlike the {110} and {111} GBs in which the valence and conduction band edges have bulk-like character. We emphasize here that the band structure of c-Si presented in the figure is that of an extended supercell of silicon and *not* of a primitive cell calculation. The periodic nature of the supercell produces a large number of shallow and flat bands in these extended structures due to zone-folding (refer to the SI for details). The band gap of the {110} GB at a 3.1 nm spacing was 1.38 eV, the {111} GB at a 3.8 nm spacing was 1.22 eV, and the single crystal Si gap was 1.17 eV. As expected, our calculated band structure for the {112} GB showed deep defect levels throughout the entire gap, giving rise to a semimetallic density of states with a small overlap between the occupied and unoccupied bands at the Fermi level, similar to that observed in high pressure phases of silicon such as BC8, and is attributed to the presence of structural deformations caused by coordination defects.[52,53] In order to further substantiate the metallic nature of the {112} GB, we computed the energy gaps of all of the GB structures using the modified Becke−Johnson[54] meta-GGA functional which is known to predict the band gaps of a wide range of elemental and compound semiconductors accurately with reasonable computational effort. The meta-GGA gaps are in good agreement with the scissor corrected PBE results for the semiconducting structures, and predicts the {112} GB to be semimetallic in line with GGA-PBE results. Analysis of the valence and conduction band charge densities for the {112} GB further confirm that the charge density is highly localized near the strained bonds of the 5-fold coordinated silicon atoms (see the Supporting Information). The computed valence and conduction band charge densities for the {110} and {111} GB cases show delocalization across the entire supercell similar to that found in crystalline silicon.

Since it is well-known that point defects are highly concentrated in the GB core, we performed DFT calculations with vacancy defects in the GBs to understand their effect on the electronic structure.[55] Using charge densities computed within GGA−PBE, we find that while a Si vacancy in {112} GBs can beneficially remove deep level states in the energy gap formed by the floating bonds, vacancies in {110} GBs produce shallow defect states close to the valance and conduction band edges[42] (see Supporting Information). We furthermore computed the formation energies for various locations of vacancy defects in {110} and {112} GBs relative to a vacancy defect in the bulk region and found that the lowest vacancy formation energy in the {112} GB (−3.13 eV) is about 1.8 eV lower than that in the {110} GB case (−1.36 eV), suggesting that the {112} GBs are thermodynamically more amenable to vacancy formation. Since in the {112} GB case the coordination defects that form at the interface cause the system to be metallic, it is conceivable that the presence of vacancies, which are thermodynamically highly favorable at this GB, could remove enough mid-gap states to restore favorable properties for PV operation. However, such a system would likely be quite challenging to control, and given the advantageous absence of deep mid-gap states in Σ_3 {110} GBs (regardless of the

presence of vacancies), as well as the fact that they show negligible electrical activity,[26] we will focus on PV devices using engineered {110} GBs in this study.

We next computed the dependence of the band gaps (E_g) of the three GB structures as a function of the spacing between them. Our results show a decreasing trend with increasing GB spacing for both the {111} and {110} semiconducting GBs (Figure 2). The {112} GB showed metallic behavior for all of the GB spacings considered here. The observed E_g behavior is consistent with the computed cohesive energy per atom of GB structures (E_c(GB)) with c-Si (E_c(Si)) as a reference, $\Delta E_c = E_c(\text{GB}) - E_c(\text{Si})$ (see Supporting Information). Our computed cohesive energy of E_c(Si) = 4.54 eV/atom for c-Si using GGA-PBE is in good agreement with previous work.[56] We see an increase in the band gap in {110} GB compared to c-Si and {111} GB, due to the difference in interface strain between the two cases. ΔE_c as well as E_g decrease with GB spacing for both the GBs, although the behavior depends upon the amount of distortion or strain at the interface and how the strain field relaxes into the crystalline lattice. As the spacing between the GBs is increased, the number of atoms inside the grains *A* and *B* increases, while the number of GB atoms remains constant, allowing the strain field to relax further. The influence of the GB on the final properties becomes weaker at larger GB spacing, as seen by a monotonic decrease of E_g in the case of the {110} GB, and is expected to converge to c-Si at much larger GB spacing. We also note that the interface strain in these GBs is not a simple tensile/compressive strain which might be applied to a bulk material, rather a mixed set of bond strains associated with the specific GB. Unsurprisingly, similar behavior is observed in the optical and electronic properties presented in the following sections.

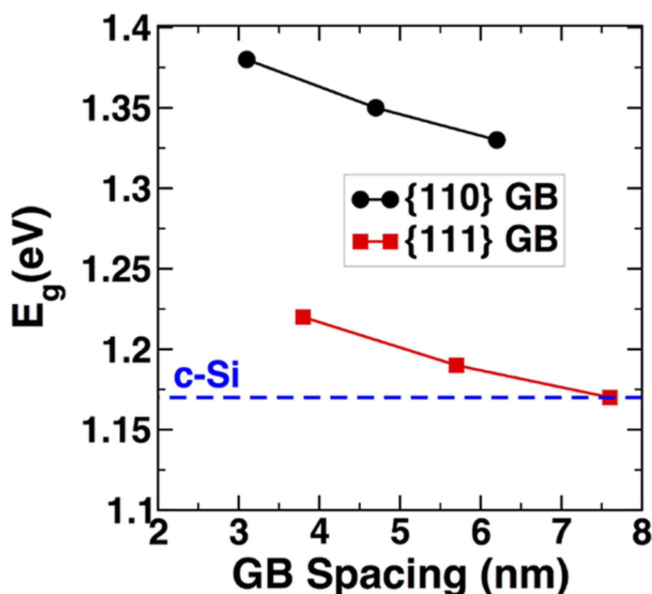

Figure 2. Variation of the energy gap, E_g, of semiconducting {110} and {111} GBs as a function of GB spacing. The {112} GB displayed metallic behavior for GB spacing up to 10 nm and is not shown. Also shown is the band gap of single crystal silicon as a reference (blue dashed line).

Optical Properties. As seen in Figure 2, the band gaps for both the {110} and {111} GBs in silicon are close to the band gap of c-Si and therefore suitable for efficient PV operation. In Figure 3 we show the computed absorption coefficient (α) as a function of excitation energy for the {110} and {111} GBs with 3 nm spacing, and c-Si and a-Si:H for comparison. The absorption coefficients of a-Si:H were averaged over 4 snapshots, obtained from the online material of ref 57, and relaxed using DFT. Since the {112} GB shows zero band gap, its optical properties were not computed. The computed α values for the {111} structure are quite similar to the case of crystalline silicon, although with a slight enhancement in the blue region of the spectrum. However, the {110} GB shows a significant increase in the optical absorption over much of the visible part of the spectrum. This is because the symmetry breaking at the interface leads to nonzero transition dipoles between the valence band and interface states located at about 2 eV above the valence band. Band decomposed charge densities show that these optically allowed transitions are localized around the GB core (see the Supporting Information). We also computed the optical properties of the {110} GB case as a function of spacing between GBs and found that even at 6.2 nm spacing the absorption coefficients are significantly higher than for c-Si in the visible region, leading to a net 16% relative increase in absorbed photons.

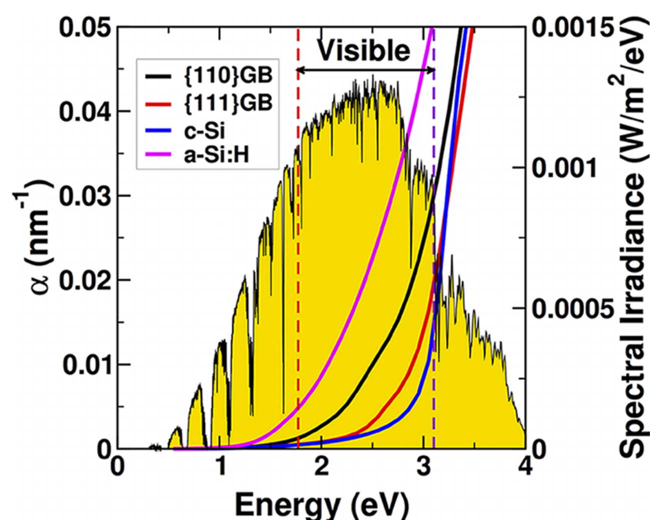

Figure 3. Computed optical absorption coefficient (α) vs energy for two GB structures and a-Si:H and c-Si for comparison. The AM1.5 solar power spectrum as a function of incident energy is shown as the shaded region.

Electronic Conductivity. We computed the electrical conductivities of *n*/*p* type c-Si and {110} GB structures as a function of doping concentration (n_e) in the range 10^{17} to 10^{20} cm^{-3} for τ = 3 fs using the Boltzmann transport equation, as shown in Figure 4. The conductivities obtained in our calculations for the single-crystal case compare well with the values previously reported.[41] Our computed conductivities for the {111} GB are almost identical to the single-crystal case and hence are not shown (see Supporting Information). In the case of the {110} GB, as expected, we find strong anisotropy in σ, with the conductivity along the direction normal to the GB plane (the *z*-axis in our unit cell) significantly lower than the in-plane conductivity. For the direction parallel to the GB plane, we predict a slight increase in σ compared to c-Si. Due to the metallic nature over the length scales considered, as with the optical absorption, the electronic conductivity of the {112} GB was not computed.

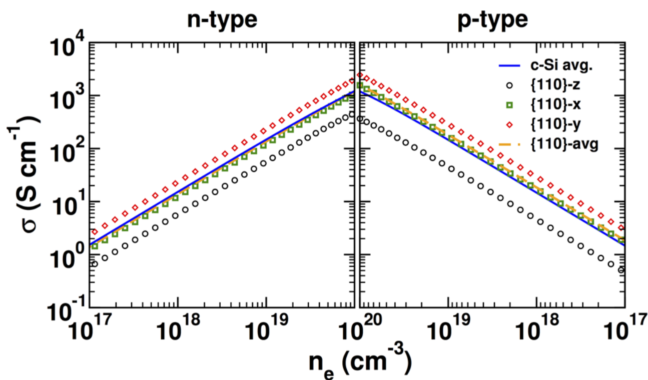

Figure 4. Electronic conductivities of the {110} GB structure with 3 nm spacing as a function of dopant concentration (n_e) for both n and p type silicon. For the GB cases the conductivity is shown separately as well as the average value, with the c-Si case shown for comparison.

A possible explanation for the anisotropic nature of σ is the symmetry breaking caused by the introduction of strain at the interface. A recent first-principles study on biaxially strained silicon showed that such strain effects can cause changes in the effective mass depending upon the type (compressive/tensile) and magnitude of strain, leading to an increase or decrease in the electronic conductivity.[58] In order to probe the anisotropic nature of σ in {110} GB, the electronic conductivity of c-Si in the presence of strain was computed. Under no-strain or in the presence of isotropic strain, the computed σ was isotropic, but under an anisotropic strain we found strong anisotropy in σ (see Supporting Information). These results further show that under anisotropic strain it is possible to observe an increase or decrease in σ along a principle direction. It is, however, interesting to note that despite the strong anisotropy, the average conductivity, given by $\sigma = (\sigma_x + \sigma_y + \sigma_z)/3$, is largely unaffected by the presence of the {110} GB when compared to c-Si. This average conductivity is critical for diffusion-dominated cells in which carriers must traverse multiple directions to be collected by front grid or finger contacts, as in most conventional c-Si devices. We emphasize here that the objective of this work is to use these GBs as an effective medium to absorb photons, generate charge carriers, and transport them along the crystalline columns and *not* across the GBs. Such columnar grains in polycrystalline CdTe have been postulated to improve solar-cell performance by constraining the hole transport along the crystalline grain bulk to the back contact rather than across the GBs.[59] Hence, the reduction of carrier mobility along the direction normal to GBs is not crucial for the functioning of GBE devices, at least for the ordered case considered here. On the contrary, the increase in conductivity along the lateral direction could actually be beneficial for current collection. We also computed the conductivity of the {110} GB case for different GB spacings and found that the average σ converges toward c-Si as the spacing between the GBs is increased, in the same manner as E_g with GB spacing.

Device Performance. Next, we utilize the results of the electronic and optical properties in full device simulations, performed for five different structures: (A) single-crystal c-Si, (B–D) {110} GB engineered silicon devices with different GB spacings, and (E) a-Si:H as the active absorber material, the schematics of which are shown in Figure 5. The thickness of active layer in devices (A–D) was chosen to be 5 microns, consistent with what is possible via current exfoliation methods.[60] The thickness of the a-Si:H device (E) was chosen

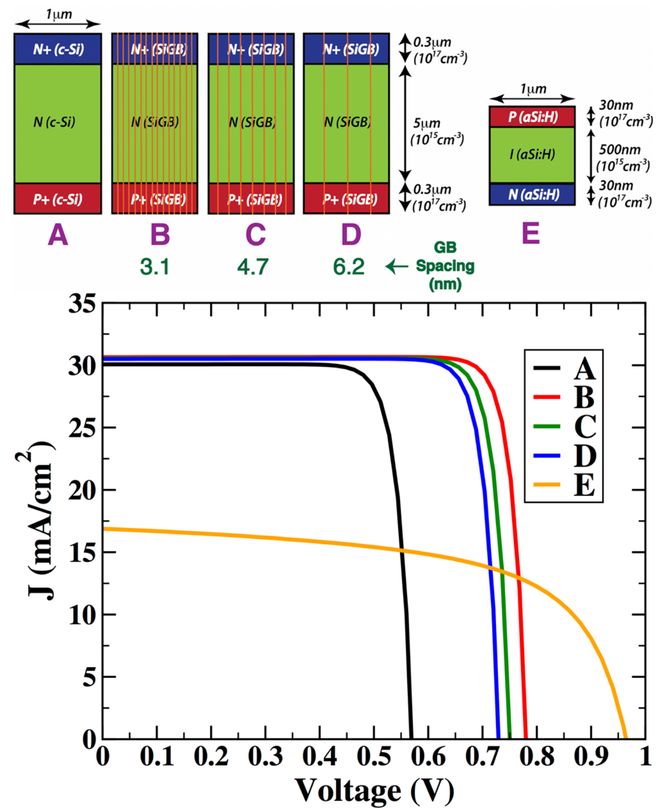

Figure 5. (Top) Schematics of three hypothetical solar cell device configurations: (A) reference c-Si device, (B–D) devices containing {110} GBs of spacings between 3.1 and 6.2 nm, and (E) device with a-Si:H as active material. The layer thickness and the corresponding carrier concentrations (inside brackets) are also shown. (Bottom) Simulated current density (J) vs voltage curves for these five devices.

to optimize the device performance, with thicker cells suffering from decreased current collection and thinner cells from limited absorption, and is included to compare to the fully disordered silicon limit. The a-Si:H material properties were obtained from ref 61. The frequency-dependent dielectric constant obtained from our DFT results was used to compute the complex refractive index, and the same was used in our wave optics simulation along with the computed (scissor-shifted) band gaps. We used electron (hole) mobility values of 1450 (500) $cm^2/(V\cdot s)$, and carrier lifetime of 10 μs for devices (A–D) in our drift-diffusion model, since our electron transport calculations discussed in the previous section did not show significant degradation in the presence of GBs. For device E, the electron and hole mobilities were 1 and 0.01 $cm^2/(V\cdot s)$, respectively, and the carrier lifetime was 0.001 μs. All device simulations were performed at 300 K and were illuminated by the AM1.5 power spectrum of 100 mW/cm^2 from the top surface.

The illuminated current density (J) is plotted as a function of the cell voltage in Figure 5. We note that the {110} GBE devices (B–D) have a slightly higher short circuit current density (J_{SC}) compared to c-Si. This is because the {110} GBE silicon has significantly higher absorption coefficients than c-Si for wavelengths in the visible region—the 16% increase in absorbed photons more than compensates for the decrease in free-carrier generation from the larger band gap, yielding a net 1% increase in current generation by device (B) relative to c-Si (A). The integrated generation rate over the entire 2-D surface

dx.doi.org/10.1021/nl501020q | Nano Lett. 2014, 14, 4943–4950

showed that the total number of charge carriers generated upon optical excitation is higher in the {110} GB devices compared to that of c-Si. Hence, {110} GBs show marginally higher short circuit current than c-Si for the device thicknesses that we have studied, but with this benefit increasing as devices are made thinner. The computed peak J_{SC} for a-Si:H is 16.9 mA/cm^2, considerably less than both the c-Si device, as well as our GB structures, due to the substantially degraded carrier transport in the fully amorphous material.

The most significant result of the GBE device simulations is the remarkable improvement in the open circuit voltage (V_{OC}) accompanying the improved absorption. Our results show that the higher band gap of {110} GBs significantly increases V_{OC} compared to silicon, which, when combined with the increased absorption, offsetting the decreased current production from the band gap increase, results in up to a 46% (relative) improvement in energy conversion efficiency. This increased voltage can be understood by considering the dependence of V_{OC} on carrier concentration:

$$V_{OC} = \frac{k_B T}{q} \ln\left[\frac{(N_A + \Delta p)\Delta n}{n_i^2}\right] \tag{2}$$

where k_B is the Boltzmann constant, T is the temperature, q is the electron charge, N_A is the doping concentration, $\Delta n = \Delta p$ is the excess carrier concentration, and n_i is the intrinsic carrier concentration.[62] The term $k_B T/q$, called the thermal voltage, is equal to 0.026 V. Since we use the same doping concentration in all our devices, n_i directly governs the V_{OC} of the device. As the carrier concentration in an intrinsic semiconductor decreases exponentially with increased band gap of the material at a given temperature, an increase in band gap can be correlated to the observed increases in V_{OC}.

Furthermore, from the Shockley–Queisser model, the temperature dependence of V_{OC} can be directly related to E_g by,

$$V_{OC} = E_g/q - CT \tag{3}$$

where C is the temperature coefficient representing the dark current characteristics of a solar cell device. Taking $C = 2 \times 10^{-3}$ V/K for c-Si,[2,63] and since the presence of {110} GBs have no significant impact on the charge mobilities, we can calculate V_{OC} to be 0.57 V, 0.78 V, 0.75 V, and 0.73 V at room temperature for devices (A → D), respectively. As expected, these values are consistent with the values obtained from the J–V curve. The key results from our device models are presented in Table 1.

One major factor that can influence the carrier mobilities in these devices is the segregation of impurities and point defects at the GB. In order to understand how the device performance is affected by changes in carrier mobilities, we performed device modeling for a range of electron and hole mobilities for the case of GB spacing 3.1 nm. We used electron mobilities in the range 1450 cm^2/(V·s) (c-Si limit) to 483 cm^2/(V·s) and hole mobilities in the range 500 cm^2/(V·s) (c-Si limit) to 167 cm^2/(V·s) for all three principal directions. We also decreased the carrier lifetimes to account for increased recombination in the presence of point defects. Although a wide range of carrier lifetime, between 0.1 μs and 1.0 μs, has been reported in the literature,[64,65] we chose the lowest value of 0.1 μs for electron and hole lifetimes for the GB structures, which is two orders of magnitude smaller than that in c-Si (10 μs). Even with this conservative model, we find that the efficiencies of GBE devices remain considerably higher than the c-Si device (Table 2).

Table 1. Key Results from the Solar Cell Device Models Shown in Figure 5 under AM1.5 Illumination

device	GB spacing (nm)	J_{SC} (mA/cm^2)	V_{OC} (mV)	fill factor (FF)	efficiency (η)	$\eta/\eta_{c\text{-Si}}$
A	none	30.07	570	0.82	14.05%	1
B	3.1	30.65	780	0.86	20.56%	1.46
C	4.7	30.55	750	0.85	19.48%	1.39
D	6.2	30.50	730	0.85	18.93%	1.35
E	none	16.9	964	0.58	9.45%	0.68

While the GBE devices studied here represent highly dense configurations of GBs by performing a second-order polynomial extrapolation of the data (columns 2 and 6) in Table 1, we estimate that it is still possible to obtain an approximately 10% relative improvement in V_{OC} and efficiency over c-Si in GBE structures with GB spacings as far as 25 nm apart. This indicates that experimentally feasible structures could not only be within reach but hold promise of further efficiency enhancements as the ability to increase the density of the engineered GBs improves.

We note that the benefits of GBE shown here are considerably different than the simple addition of a-Si:H into an otherwise crystal silicon material. This is because the latter is known to form mid-gap and band tail states, both of which can severely impact carrier mobility even along the crystalline grains, as well as increase the probability of carrier recombination. In contrast, the GBE material discussed here is a controlled way of introducing disorder in silicon - while not all GBs are beneficial for PV, we have shown that the proper selection (such as the {110} GB here) could aid in the energy conversion process. This suitable choice of GB combined with its ordered layering of 3–20 nm offers a way to balance the incorporation of advantageous properties of amorphous silicon while avoiding the degraded electronic transport of a fully amorphous system.

Conclusions. We have shown that, by understanding the role of GBs on the optical and electronic properties of c-Si, it is possible to design novel nanostructured material architectures with improved photovoltaic properties. We find that the {111} twin boundaries have minimal atomic rearrangement at the interface, with changes to the electronic structure being relatively insignificant, while the {112} GBs are associated with bonding defects that lead to metallic behavior. The {110} GBs, however, possess an increased band gap relative to c-Si, which alone is shown to yield relative V_{OC} improvements of 28% to 36% over c-Si, for 5 micron thick cells and GB spacings of 6.2 to 3.1 nm, respectively.

For the {110} GB, we additionally find a significant improvement in the optical absorption over much of the visible spectrum, without degradation in the overall electronic conductivity relative to c-Si. The absorption of the GBE material is shown to yield relative J_{SC} improvements of 1.4% to 1.9% over c-Si even after compensating for the decreased accessible energy range due to the increased band gap, again for the respective GB spacings of 6.2 to 3.1 nm, in 5 μm thick cells. As the push toward ultrathin, kerfless wafer processing allows c-Si substrates to be made continually thinner, this enhanced absorption becomes increasingly advantageous. At reduced GB densities (20 nm spacing) and for thick devices (∼100% absorption above E_g), we still predict 4% relative efficiency improvements over c-Si, due to the increased band gap. This

Table 2. Results from the Solar Cell Device Models for Devices with GB Spacing 3.1 nm under AM1.5 Illumination for Different Carrier Mobilities and Carrier Lifetime of 0.1 μs^a

device	μ_e	μ_h	J_{SC} (mA/cm^2)	V_{OC} (mV)	fill factor (FF)	efficiency (η)
F	μ_e(Si)	μ_h(Si)	29.09	775	0.85	19.38%
G	μ_e(Si)*2/3	μ_h(Si)*2/3	28.36	777	0.85	18.95%
H	μ_e(Si)*1/2	μ_h(Si)*1/2	27.66	779	0.85	18.53%
I	μ_e(Si)*2/5	μ_h(Si)*2/5	26.99	780	0.85	18.10%
J	μ_e(Si)*1/3	μ_h(Si)*1/3	26.36	782	0.85	17.73%

[a] μ_e(Si) = 1450 cm^2/V·s and μ_h(Si) = 500 cm^2/V·s are the mobilities in c-Si.

combination of the enhanced absorption for thin materials, as well as the enhanced band gap for dense GB arrangements, could make these GBE structures attractive candidates for the design of future novel and efficient solar cells.

■ ASSOCIATED CONTENT

Supporting Information

Details of methodology, atomic structure, zone folding in extended silicon supercells, GGA vs meta-GGA band structures, valence and conduction band charge densities for the GB structures, cohesive energy, effect of GB spacing on optical absorption, absorptive power of GB materials compared to c-Si and a-Si:H, computed electronic conductivities of {110} GB as a function of GB spacing, and electronic conductivity of c-Si under strain. This material is available free of charge via the Internet at http://pubs.acs.org.

■ AUTHOR INFORMATION

Corresponding Author

*E-mail: jcg@mit.edu.

Notes

The authors declare no competing financial interest.

■ ACKNOWLEDGMENTS

This work was supported by grants from King Fahd University of Petroleum and Minerals (KFUPM) in Dhahran, Saudi Arabia under Project No. R1-CE-08. The authors acknowledge Teragrid for computational resources, supported by the National Science Foundation under Grants TG-DMR090027 and TG-DMR110027. R.R. acknowledges Dr. Joo-Hyoung Lee, GIST, Korea and Dr. Engin Durgun, Bilkent University, Turkey, for their help during this project.

■ REFERENCES

(1) The State of U.S. Manufacturing; *PV News*, January, 2012; Greentech Media Research; Vol. *31*, pp 1−28.
(2) Shockley, W.; Queisser, H. J. *J. Appl. Phys.* **1961**, *32*, 510−519.
(3) Liang, J.; Schiff, E. A.; Guha, S.; Yan, B.; Yang, J. *Appl. Phys. Lett.* **2006**, *88*, 063512.
(4) Staebler, D. L.; Wronski, C. R. *Appl. Phys. Lett.* **1977**, *31*, 292−294.
(5) Street, R. *Hydrogenated Amorphous Silicon*; Cambridge University Press: Cambridge, U.K., 1991; pp 390−391.
(6) Chen, H.; Gullanar, M.; Shen, W. *J. Cryst. Growth* **2004**, *260*, 91−101.
(7) Reynolds, S. *J. Optoelectron. Adv. Mater.* **2009**, *11*, 1086−1092.
(8) NREL Efficiency Chart. http://www.nrel.gov/ncpv/images/efficiency_chart.jpg (May 11, 2014).
(9) Bruhne, K.; Schubert, M.; Kohler, C.; Werner, J. *Thin Solid Films* **2001**, *395*, 163−168.
(10) Yue, G.; Yan, B.; Ganguly, G.; Yang, J.; Guha, S.; Teplin, C. W. *Appl. Phys. Lett.* **2006**, *88*, 263507.
(11) Pearce, J. M.; Podraza, N.; Collins, R. W.; Al-Jassim, M. M.; Jones, K. M.; Deng, J.; Wronski, C. R. *J. Appl. Phys.* **2007**, *101*, 114301.
(12) Visoly-Fisher, I.; Cohen, S. R.; Ruzin, A.; Cahen, D. *Adv. Mater.* **2004**, *16*, 879−883.
(13) Bosio, A.; Romeo, N.; Podestà, A.; Mazzamuto, S.; Canevari, V. *Cryst. Res. Technol.* **2005**, *40*, 1048−1053.
(14) Li, C.; Wu, Y.; Poplawsky, J.; Pennycook, T. J.; Paudel, N.; Yin, W.; Haigh, S. J.; Oxley, M. P.; Lupini, A. R.; Al-Jassim, M.; Pennycook, S. J.; Yan, Y. *Phys. Rev. Lett.* **2014**, *112*, 156103.
(15) Nowell, M. M.; Wright, S. I.; Scarpulla, M. A.; Compaan, A. D.; Liuc, X.; Paudel, N. R.; Wieland, K. A. Physical and Failure Analysis of Integrated Circuits (IPFA), 19th IEEE International Symposium on the, July 2-6, 2012, Singapore; pp 1-7; DOI: 10.1109/IPFA.2012.6306331.
(16) Kohyama, M.; Yamamoto, R. *Phys. Rev. B* **1994**, *49*, 17102−17117.
(17) Morris, J. R.; Fu, C. L.; Ho, K. M. *Phys. Rev. B* **1996**, *54*, 132−138.
(18) Watanabe, T.; Kido, K.; Tsurekawa, S.; Kawahara, K. *Mater. Sci. For.* **2007**, *558−559*, 843−850.
(19) Watanabe, T.; Tsurekawa, S.; Zhao, X.; Zuo, L. In *Microstructure and Texture in Steels*; Haldar, A., Suwas, S., Bhattacharjee, D., Eds.; Springer: London, 2009; pp 43−82.
(20) Jeon, J.-H.; Park, K.-C.; Lee, M.-C.; Han, M.-K. *J. Non-Cryst. Solids* **2000**, *266−269*, 645−649.
(21) Huang, W. L.; Ge, W.; Li, C.; Hou, C.; Wang, X.; He, X. *Comput. Mater. Sci.* **2012**, *58*, 38−44.
(22) Suvitha, A.; Venkataramanan, N. S.; Sahara, R.; Mizuseki, H.; Kawazoe, Y. *Jpn. J. Appl. Phys.* **2010**, *49*, 04DP02.
(23) Feng, C. B.; Nie, J. L.; Zu, X. T.; Al-Jassim, M. M.; Yan, Y. *J. Appl. Phys.* **2009**, *106*, 113506.
(24) Sawada, H.; Ichinose, H.; Kohyama, M. *J. Phys.: Condens. Matter* **2007**, *19*, 026223.
(25) Yan, Y.; Jones, K.; Jiang, C.; Wu, X.; Noufi, R.; Al-Jassim, M. *Phys. B (Amsterdam, Neth.)* **2007**, *401−402*, 25−32.
(26) Wang, Z.-J.; Tsurekawa, S.; Ikeda, K.; Sekiguchi, T.; Watanabe, T. *Interface Sci.* **1999**, *7*, 197−205.
(27) Ogawa, H. *Mater. Trans.* **2006**, *47*, 2706−2710.
(28) Kresse, G.; Furthmuller, J. *Comput. Mater. Sci.* **1996**, *6*, 15−50.
(29) Blöchl, P. E. *Phys. Rev. B* **1994**, *50*, 17953−17979.
(30) Kresse, G.; Joubert, D. *Phys. Rev. B* **1999**, *59*, 1758−1775.
(31) Perdew, J. P.; Burke, K.; Ernzerhof, M. *Phys. Rev. Lett.* **1996**, *77*, 3865−3868.
(32) Perdew, J. P.; Burke, K.; Ernzerhof, M. *Phys. Rev. Lett.* **1997**, *78*, 1396−1396.
(33) Vojta, T.; Mertig, I.; Zeller, R. *Phys. Rev. B* **1992**, *46*, 15761−15766.
(34) Thonhauser, T.; Scheidemantel, T. J.; Sofo, J. O. *Appl. Phys. Lett.* **2004**, *8*, 588−590.
(35) Yang, J.; Li, H.; Wu, T.; Zhang, W.; Chen, L.; Yang, J. *Adv. Funct. Mater.* **2008**, *18*, 2880−2888.
(36) Singh, D. J. *Phys. Rev. B* **2010**, *81*, 195217.
(37) May, A. F.; Singh, D. J.; Snyder, G. J. *Phys. Rev. B* **2009**, *79*, 153101.
(38) Lee, M.-S.; Poudeu, F. P.; Mahanti, S. D. *Phys. Rev. B* **2011**, *83*, 085204.

(39) Ashcroft, N. W.; Mermin, D. N. *Solid State Phys.* **2009**, 244−251.
(40) Gaymann, A.; Geserich, H. P.; Löhneysen, H. v. *Phys. Rev. B* **1995**, *52*, 16486−16493.
(41) Weber, L.; Gmelin, E. *Appl. Phys. A: Mater. Sci. Process.* **1991**, *53*, 136−140.
(42) Sakaguchi, N.; Ichinose, H.; Watanabe, S. *Mater. Trans.* **2007**, *48*, 2585−2589.
(43) Sakaguchi, N.; Miyake, M.; Watanabe, S.; Takahashi, H. *Mater. Trans.* **2011**, *52*, 276−279.
(44) Kholod, A.; Borisenko, V.; Saúl, A.; d'Avitaya, F. A.; Fuhr, J. *Opt. Mater.* **2001**, *17*, 61−63.
(45) Ke, S.-h.; Zhang, K.-m.; Xie, X.-d. *Phys. Rev. B* **1997**, *55*, 5124−5128.
(46) Zhao, X.; Wei, C. M.; Yang, L.; Chou, M. Y. *Phys. Rev. Lett.* **2004**, *92*, 236805.
(47) Ng, M.-F.; Sullivan, M. B.; Tong, S. W.; Wu, P. *Nano Lett.* **2011**, *11*, 4794−4799.
(48) Zhang, L.; d'Avezac, M.; Luo, J.-W.; Zunger, A. *Nano Lett.* **2012**, *12*, 984−991.
(49) Boykin, T. B.; Klimeck, G. *Phys. Rev. B* **2005**, *71*, 115215.
(50) Ku, W.; Berlijn, T.; Lee, C.-C. *Phys. Rev. Lett.* **2010**, *104*, 216401.
(51) Ferraro, E.; Hogan, C.; Palummo, M.; Del Sole, R. *Phys. Status Solidi B* **2012**, *249*, 1148−1154.
(52) Malone, B. D.; Sau, J. D.; Cohen, M. L. *Phys. Rev. B* **2008**, *78*, 035210.
(53) Malone, B. D.; Sau, J. D.; Cohen, M. L. *Phys. Rev. B* **2008**, *78*, 161202.
(54) Tran, F.; Blaha, P. *Phys. Rev. Lett.* **2009**, *102*, 226401.
(55) Dudeck, K. J.; Walters, W. D.; Knights, A. P.; Coleman, P. G. *J. Phys. D* **2008**, *41*, 055102.
(56) Farid, B.; Godby, R. W. *Phys. Rev. B* **1991**, *43*, 14248−14250.
(57) Johlin, E.; Wagner, L. K.; Buonassisi, T.; Grossman, J. C. *Phys. Rev. Lett.* **2013**, *110*, 146805.
(58) Hinsche, N.; Mertig, I.; Zahn, P. *J. Phys.: Cond. Mater.* **2011**, *23*, 295502.
(59) Visoly-Fisher, I.; Cohen, S.; Gartsman, K.; Ruzin, A.; Cahen, D. *Adv. Funct. Mater.* **2006**, *16*, 649−660.
(60) Saha, S.; Hilali, M. M.; Onyegam, E. U.; Sarkar, D.; Jawarani, D.; Rao, R. A.; Mathew, L.; Smith, R. S.; Xu, D.; Das, U. K.; Sopori, B.; Banerjee, S. K. *Appl. Phys. Lett.* **2013**, *102*, 163904.
(61) Schropp, R.; Zeman, M. *Amorphous and microcrystalline silicon solar cells: Modeling, Materials and Device Technology*; Kluwer: Amsterdam, 1998; pp 47 and 183.
(62) Sinton, R. A.; Cuevas, A. *Appl. Phys. Lett.* **1996**, *69*, 2510−2512.
(63) Tayagaki, T.; Hoshi, Y.; Usami, N. *Sci. Rep.* **2013**, *3*, 2703.
(64) Metzger, W. K. *Sol. Energy Mater. Sol. Cells* **2008**, *92*, 1123−1135.
(65) Sakata, I.; Hayashi, Y.; ichi Ishii, K.; Takahashi, T.; Yamanaka, M. *Jpn. J. Appl. Phys.* **1986**, *25*, L328−L330.